A Stress-Free and Textured GaP Template on Silicon for Solar Water Splitting

Ida Lucci, Simon Charbonnier, Maxime Vallet, Pascal Turban, Yoan Léger, Tony Rohel, Nicolas Bertru, Antoine Létoublon, Jean-Baptiste Rodriguez, Laurent Cerutti, et al.

ADVANCED FUNCTIONAL MATERIALS

Postfach 10 11 61
69451 Weinheim
Germany
Courier services:
Boschstraße 12
69469 Weinheim
Germany
Tel.: (+49) 6201 606 531
Fax: (+49) 6201 606 500
E-mail: afm@wiley.com

WILEY-VCH

Dear Author,

Please correct your galley proofs carefully and return them no more than four days after the page proofs have been received.

Please limit corrections to errors already in the text; cost incurred for any further changes or additions will be charged to the author, unless such changes have been agreed upon by the editor.

The editors reserve the right to publish your article without your corrections if the proofs do not arrive in time.

Note that the author is liable for damages arising from incorrect statements, including misprints.

Please note any queries that require your attention. These are indicated with a Q in the PDF and a question at the end of the document.

Reprints may be ordered by filling out the accompanying form.

Return the reprint order form by fax or by e-mail with the corrected proofs, to Wiley-VCH : **afm@wiley.com**

To avoid commonly occurring errors, **please ensure that the following important items are correct** in your proofs (please note that once your article is published online, no further corrections can be made):

- **Names** of all authors present and spelled correctly
- **Titles** of authors correct (Prof. or Dr. only: please note, Prof. Dr. is not used in the journals)
- **Addresses** and **postcodes** correct
- **E-mail address** of corresponding author correct (current email address)
- **Funding bodies** included and grant numbers accurate
- **Title** of article OK
- All **figures** included
- **Equations** correct (symbols and sub/superscripts)

Corrections should be made directly in the PDF file using the PDF annotation tools. If you have questions about this, please contact the editorial office. The corrected PDF and any accompanying files should be uploaded to the journal's Editorial Manager site.

Author Query Form

WILEY

Journal ADFM

Article adfm201801585

Dear Author,

During the copyediting of your manuscript the following queries arose.

Please refer to the query reference callout numbers in the page proofs and respond to each by marking the necessary comments using the PDF annotation tools.

Please remember illegible or unclear comments and corrections may delay publication.

Many thanks for your assistance.

Query No.	Description	Remarks
Q1	Please confirm that forenames/given names (red) and surnames/family names (green) have been identified correctly.	
Q2	Please provide the highest academic title (either Dr. or Prof.) for all authors, where applicable.	
Q3	Please provide postal code in affiliation 4.	
Q4	Please check all equations have been correctly typeset.	
Q5	Please verify year, volume and page number in ref. (28).	
Q6	Please verify page number in ref. (44).	
Q7	Please add the publisher location in ref. (51).	
Q8	The citation for refs. (54–57) is missing in the main text. Please cite reference at the appropriate place.	

Author: Please confirm that Funding Information has been identified correctly.

Please confirm that the funding sponsor list below was correctly extracted from your article: that it includes all funders and that the text has been matched to the correct FundRef Registry organization names. If a name was not found in the FundRef registry, it may not be the canonical name form, it may be a program name rather than an organization name, or it may be an organization not yet included in FundRef Registry. If you know of another name form or a parent organization name for a "not found" item on this list below, please share that information.

FundRef Name	FundRef Organization Name
French National Research Agency	French National Research Agency Project ANTIPODE
Project ANTIPODE	

Water Splitting

I. Lucci, S. Charbonnier,
M. Vallet, P. Turban, Y. Léger,
T. Rohel, N. Bertru, A. Létoublon,
J.-B. Rodriguez, L. Cerutti, E. Tournié,
A. Ponchet, G. Patriarche, L. Pedesseau,*
C. Cornet*.....1801585

A Stress-Free and Textured GaP Template on Silicon for Solar Water Splitting

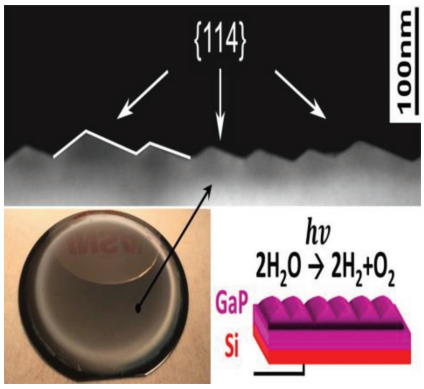

A large-scale stress-free textured GaP template monolithically integrated on Si is by surface energy engineering, for water-splitting applications. The stability of GaP{114} facets is examined thermodynamically. The benefits of using a textured (114)A GaP/Si template for water-splitting applications, in terms of surface gain, band lineups, and ohmic contacts are finally discussed.

ADVANCED FUNCTIONAL MATERIALS
www.afm-journal.de

A Stress-Free and Textured GaP Template on Silicon for Solar Water Splitting

Ida Lucci, Simon Charbonnier, Maxime Vallet, Pascal Turban, Yoan Léger, Tony Rohel, Nicolas Bertru, Antoine Létoublon, Jean-Baptiste Rodriguez, Laurent Cerutti, Eric Tournié, Anne Ponchet, Gilles Patriarche, Laurent Pedesseau,* and Charles Cornet*

This work shows that a large-scale textured GaP template monolithically integrated on Si can be developed by using surface energy engineering, for water-splitting applications. The stability of (114)A facets is first shown, based on scanning tunneling microscopy images, transmission electron microscopy, and atomic force microscopy. These observations are then discussed in terms of thermodynamics through density functional theory calculations. A stress-free nanopatterned surface is obtained by molecular beam epitaxy, composed of a regular array of GaP (114)A facets over a 2 in. vicinal Si substrate. The advantages of such textured (114)A GaP/Si template in terms of surface gain, band lineups, and ohmic contacts for water-splitting applications are finally discussed.

1. Introduction

Solar photoelectrochemical (PEC) water-splitting devices have attracted interest for decades with the ultimate objective to convert and store the solar energy into clean hydrogen fuel[1,2] at a lower production cost and environmental impact. Indeed, more than 90% of the hydrogen production is today made by steam methane reforming which releases carbon monoxide/dioxide and heat into the atmosphere while global warming is an issue.[3] The conversion of solar energy into hydrogen production through a water-splitting process assisted by photosemiconductor catalysts[4,5] is definitely the most promising technology for the near future with potentially plethora of hydrogen provided in a clean and sustainable manner. Many recent proposals deal with the use of the GaP semiconductor as a photoelectrode in PEC devices,[6] especially because its bandgap (2.26 eV) is larger than the 1.73 eV photopotential needed for water splitting.[7] Using this idea, demonstrations of GaP-based PEC devices[8–11] and descriptions of the physics/chemistry of the standard GaP surface,[12] its interaction with water[13,14] and hydrogen generation[15] were reported. To enhance conversion efficiency of GaP-based PEC devices, strategies like surface functionalization,[10] use of plasmon resonant nanostructures,[16] or integration of nanowires[17] were considered. Meanwhile, it was demonstrated recently that the texturation of surfaces at the electrode level greatly enhances the efficiency of $BiVO_4$ photoanodes in PEC devices.[18] Structuration of semiconductor surfaces can be performed by lithography techniques,[19] chemical processes,[20,21] nanowires, or by a self-organization during the epitaxial process of the material itself.[22] This last approach is usually driven by crystal strain-relief processes; it simplifies the postgrowth device processing but does not offer large degrees of freedom,

I. Lucci, Dr. Y. Léger, T. Rohel, Prof. N. Bertru, Dr. A. Létoublon, Dr. L. Pedesseau, Dr. C. Cornet
Univ Rennes
INSA Rennes
CNRS
Institut FOTON - UMR 6082
F-35000, Rennes, France
E-mail: laurent.pedesseau@insa-rennes.fr; charles.cornet@insa-rennes.fr

S. Charbonnier, Dr. P. Turban
Univ Rennes
CNRS
IPR (Institut de Physique de Rennes) – UMR 6251
F-35000 Rennes, France

Dr. M. Vallet, Dr. A. Ponchet
CEMES-CNRS
Université de Toulouse
UPS
29 rue Jeanne Marvig
BP 94347 Toulouse, Cedex 04, France

Dr. J.-B. Rodriguez, Dr. L. Cerutti, Prof. E. Tournié
IES
Univ. Montpellier
CNRS
Montpellier, France

Dr. G. Patriarche
Centre de Nanosciences et de Nanotechnologies
site de Marcoussis
CNRS
Université Paris Sud
Université Paris Saclay
route de Nozay 91460 Marcoussis, France

DOI: 10.1002/adfm.201801585

while keeping a crystal quality compatible with operating devices. The need for a scalable PEC device, in view of its very large-scale integration was also pointed out.[23] In this regard, GaP presents several advantages. Among them, its monolithic integration on silicon leads to a high crystal quality, due to the low lattice mismatch between GaP and Si (0.36% at room temperature).[24]

In this work, we show that a large-scale textured GaP template monolithically integrated on Si can be developed by using surface energy engineering. We first evidence the remarkable stability of (114)A GaP facets, based on scanning tunneling microscopy (STM) images, transmission electron microscopy (TEM), and atomic force microscopy (AFM). Facets stabilization is also discussed in terms of thermodynamics through density functional theory (DFT) calculations. We then demonstrate that a stress-free nanopatterned surface can be grown by molecular beam epitaxy (MBE), composed of a regular array of (114)A facets over a 2 in. vicinal Si substrate. We finally assess the potentiality of the textured (114)A GaP/Si template toward water-splitting applications.

2. Results and Discussions

2.1. Textured GaP Surface on Si(001) 6°-off

To design efficiently a textured semiconductor surface, a good knowledge of the non-(001) most stable surfaces is needed. Stable facets are easily identified in stress-induced nanostructures, such as quantum dots.[25] But it is also possible to use stress-free surface structures whose formation is highly correlated to emerging defects, for instance, antiphase domains (APDs) separated by emerging antiphase boundaries (APBs).[26] In this regard, a 10 nm thick GaP has been grown on a freshly prepared HF-last Si(001) substrate. Before starting the GaP/Si(001) growth process, the silicon substrate has been annealed at 800 °C in order to desorb the hydrogen. With this preparation (without Si buffer layer), the Si surface remains bi-domain. After that, the GaP was grown at 350 °C by molecular beam epitaxy using migration enhanced epitaxy (see refs. [24,27,28] for growth procedure and apparatus description). This layer was further annealed at 500 °C. An amorphous As capping layer was then deposited at cryogenic temperatures to avoid any air contamination during transfer to the STM ultrahigh vacuum (UHV) chamber, as explained in refs. [25,29]

Figure 1a shows the STM image of the 10 nm thick GaP/Si surface. Two antiphase domains are observed. Each domain is first characterized by a large (001) surface where the dimers are aligned along the local [1-10] directions. Different facets can be identified at the boundaries where the two domains coalesce. Among the different facets observed, {136}, {113}, and (114)A and B are clearly identified by their angle and surface reconstructions. Especially, as highlighted in Figure 1a, the surface is quantitatively mainly covered by {114} and (001) facets. The stability of GaAs{114}A or InGaAs {114}A facets was already widely discussed in the literature.[30–32] The work of Yamada et al., who performed STM investigations, showed low kink density and a highly uniform surface structure for the GaAs{114}A facets. Márquez et al. also observed a well-ordered GaAs(114)A$\alpha 2(2\times 1)$ reconstruction, discussing its relative stability with respect to the GaAs(001)A$\beta 2(2\times 4)$ one with ab initio calculations.

To promote {114}A surface texturation, we need thermodynamic conditions where the energy of the {114}A faceted

Ida Lucci received the B.Sc. and M.Sc. degrees in electrical engineering from University of Naples "Federico II," Italy, in 2012 and 2015, respectively. In 2015, she started studying the thermal management of integrated laser devices. She is now working toward the Ph.D. degree at FOTON Laboratory at INSA, Rennes, France. Her research focuses on the pseudomorphic integration of III–V semiconductors on silicon, understanding the impact of the silicon surface at the atomic scale on the crystal growth of III–V compounds.

Laurent Pedesseau obtained his M.Sc. in condensed matter from the University of Montpellier in 2001. In 2004, he received his Ph.D. in physics from the University of Toulouse for atomistic empirical simulations applied to civil engineering materials. In 2013, he was appointed as assistant professor at FOTON Institute (INSA Rennes) to work on III–V semiconductor nanostructures for silicon photonics, hybrid-perovskites for photovoltaics, and optoelectronic device simulations for optical telecommunication.

Charles Cornet received his Ph.D. degree in physics from Institut National des Sciences Appliquées, Rennes, France, in 2006 for his contribution to the understanding of electronic, optical, and dynamic properties of coupled self-assembled InAs/InP quantum dots. Since 2007, he is assistant professor Hab. at FOTON laboratory, specialist of MBE material growth, structural and optical properties of III–V semiconductor nanostructures and devices, and their integration on silicon. Since 2017, he leads the "Optoelectronics, Heteroepitaxy and Materials" research group of the FOTON Institute.

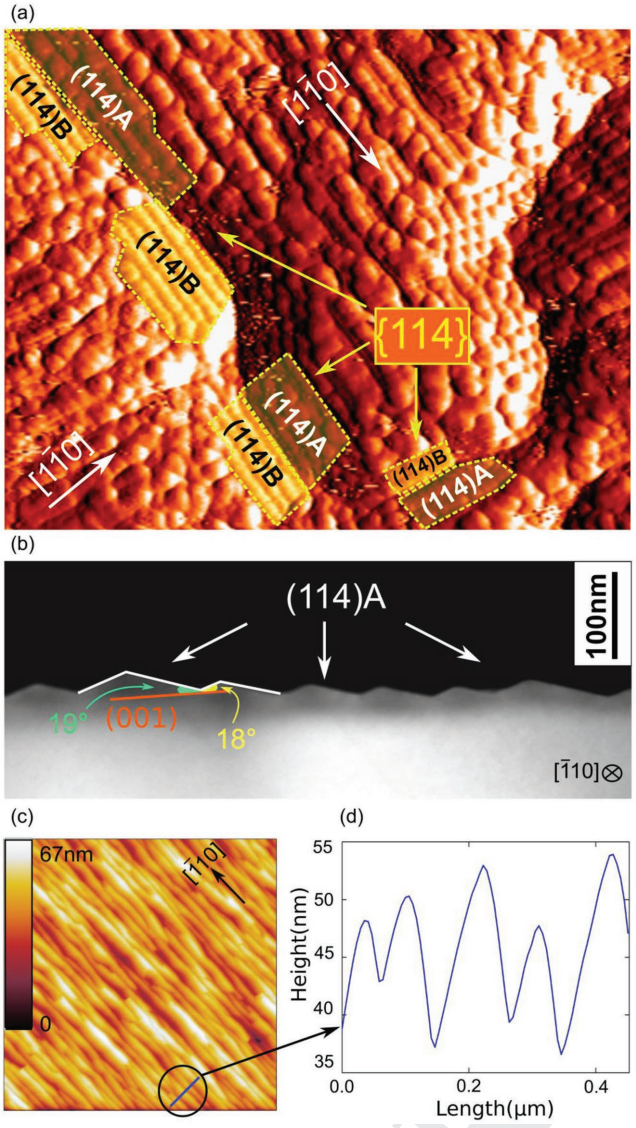

Figure 1. a) 25 × 30 nm^2 STM image of a bi-domain 10 nm thick GaP on Si(001) evidencing the presence of numerous (114)A and B facets at the antiphase boundaries edges. b) TEM image of 1 µm thick GaP on Si 6°-off. c) 3 µm × 3 µm AFM image of the surface of the same sample as (b). (d) A profile taken by small region of the AFM image. TEM and AFM observations show the (114)A faceting of the GaP surface.

surface is lower than the {001} one, that is, by developing a surface energy engineering approach. To this aim, a 1 µm thick GaP sample was grown on a vicinal Si (001)-6°-off substrate. Corresponding TEM and AFM images and profiles are shown in Figure 1a,c,d. In this sample, most of the antiphase domains (APDs) were annihilated within the first 20 nm, by using AlGaP filtering layers, as demonstrated in the TEM image of ref. [24] The remaining GaP is grown at 580 °C, with an intermediate beam equivalent pressure (BEP) V/III ratio of 4. The crystal growth was monitored in situ using reflection high-energy electron diffraction (RHEED) experiments. The 1 µm thickness is well above the critical thickness, and X-ray diffraction experiments (not shown here) reveal an overall full relaxation of the GaP crystal. Figure 1b shows the ⟨110⟩ cross-sectional TEM image of the sample. The surface presents a saw-tooth profile along the lateral ⟨110⟩ direction. All facets have an angle with the (001) plane between 18° and 20°, close to the theoretical angle calculated for the {114} facets, that is, $\theta = 19.48°$. The average distance between two maxima is 100 nm with a dispersion of 40%. In the TEM image, left-oriented and right-oriented (114)A facets present different widths. The saw-tooth asymmetry allows compensating the 6°-miscut of the silicon substrate. It is important to note that (001) facets are completely missing. We also point out that (114) facets are parallel to the step edges direction of the vicinal silicon substrate, suggesting that the direction of the substrate miscut determines the dominant polarity of the grown GaP. We also note that emerging dislocation density remains low on this relaxed sample, because of the low lattice mismatch.

Interestingly, these facets were also observed by RHEED. During the growth a thin and streaky pattern, orientated with a 15°–20° angle from the conventional (001) usual RHEED diffraction direction was observed. Even if the RHEED apparatus used in this study does not allow to determine precisely the observed reconstruction, diffraction lines were found to be remarkably thin as compared to the usual (2 × 4) (001) GaP ones, suggesting a good planarity of the facets. We also note here that similar observations were done on more than ten different samples, grown in the same conditions, showing the reproducibility of the process.

The resulting surface pattern is also highlighted in Figure 1c where a plan-view AFM image is shown. The corresponding saw-tooth profile is also given in Figure 1d. Here, the measured profile is smoother than the one obtained with TEM measurements, because of AFM tip convolution effects. A strong anisotropy of the surface structuration is revealed. The typical length of one facet is larger than 2 µm, to be compared to the 100 nm average distance between saw-tooth profile. This confirms that antiphase domains have been well annihilated, over the observed 3 × 3 µm^2 surface. The morphologies observed by TEM and AFM thus clearly show that in these conditions the (001) GaP surface is unstable against (114)A faceting. It experimentally suggests that the energy surface of the (114)A surface over $\cos(\theta)$ is here lower than the (001) surface energy. Interestingly, it is worth mentioning that a similar growth on the GaP native substrate does not lead to any {114} surface structuration indicating that growth on the vicinal silicon substrate impacts the surface properties.

Beyond the use of a vicinal substrate, we have also observed that changing group-V atmosphere above the surface on a nominal GaP substrate, can be another strategy for surface energy engineering promoting a textured-surface formation on GaP. Indeed, the textured behavior was obtained by simply exposing the GaP surface under Sb atmosphere (Figure S1, Supporting Information). Besides III–Vs systems, a similar surface energy engineering strategy has also been developed to control the growth morphology by promoting a 2D–3D transition for growing self-assembled II–VI and nitride quantum dots (QDs).[33–35] Indeed, in both the cases, the SK transition was interpreted as a surface energy change due to a saturation of the dangling bonds by changing the species exposure. Nevertheless, all the present observations demonstrate that there is a real competition between the growth of a (001) surface and the (114)A faceting.

2.2. Surface Energies Computed by DFT

The stability of the {114} facets is discussed thermodynamically in the following. The DFT is used to estimate the surface energy of the (001) polar GaP surface and the (114) A and B polar GaP surfaces. Every surface considered in this work fulfills the electron counting model (ECM).[36] For both (001) and {114} facets, P-rich and Ga-rich reconstructions are considered. In the case of the nonpolar GaP(001) surface, two different (2×4) reconstructions are computed. For the Ga-rich GaP(001) surface, the GaP(001)md(2×4)[37,38] reconstruction (where md stands for mixed dimers) is assumed. This reconstruction is often considered for Ga-rich conditions in the literature.[12,14,39] For the P-rich GaP(001) surface, different stable structures were proposed[40] and H-passivated reconstructions were considered for metal–organic chemical vapor deposition growth or in the context of water-splitting applications.[14,41,42] In this study where samples are grown by MBE, we use a simple anion (P)-rich GaP(001) surface that fulfills the ECM criteria as proposed for GaAs.[36] We believe that any change of this reconstruction does not qualitatively affect the main conclusions of the study.

For the polar GaP(114) surfaces, two types of (2×1) reconstructions have been simulated: the Ga-rich GaP(114)A-$\alpha 2(2 \times 1)$ and the P-rich GaP(114)B-$\alpha 2(2 \times 1)$ which are similar to the ones already thoroughly investigated for the GaAs(114).[31,43,44] While simple subtraction methods can be used to compute surface energies of nonpolar surfaces such as the GaP(001) ones, fictitious hydrogen methods have to be used to compute A and B polar surfaces independently with a good accuracy (see the Supporting Information for a detailed surface structures description). In the case of nonstoichiometric surfaces such as the (001) surfaces considered here, surface atoms are in equilibrium with a reservoir, therefore the computed surface energy strongly depends on the chemical potential μ and the surface stoichiometry $\Delta N = N_P - N_{Ga}$.[45]

The general equation used to determine the surface energies is

$$\gamma_{surface} A = E_{slab} - \sum_i \mu_i N_i \quad (1)$$

where $\gamma_{surface}$ is the surface energy, A the surface area, E_{slab} is the slab energy calculated by DFT, μ_i is the chemical potential of the species i (where i is Ga or P), and N_i is the number of particles of the species i of the slab. The temperature dependence is ignored because the contributions tend to cancel for free-energy differences as claimed for the GaAs material in a previous study.[46]

In **Figure 2**, the surface energies versus the chemical potential variations are shown for GaP(001) and GaP(114) surfaces.

The slope of the P-rich GaP(001)(2×4) and Ga-rich GaP(001)md(2×4) surface energy curves (the green and blue one, respectively) is inherent to their stoichiometry. Indeed, both GaP(001)(2×4) surfaces are nonstoichiometric, that is, $N_P \neq N_{Ga}$. In particular, we find $\Delta N = 16$ for the P-rich GaP(001) (2×4) case while $\Delta N = 8$ for the Ga-rich GaP(001)md(2×4) one. Instead, the GaP(114)A-$\alpha 2(2 \times 1)$ and the GaP(114)B-$\alpha 2(2 \times 1)$ surfaces are stoichiometric ($\Delta N = 0$). Consequently, their surface energies (the pink and brown curve, respectively) are constant with the chemical potential. Their values are about 59.9 and 67.3 meV Å^{-2}, respectively.

The chemical potential μ_i has to vary between two extremes thermodynamic conditions: Ga-rich limit (i.e., bulk Ga will form preferentially) and P-rich limit (bulk P will form preferentially). In particular, the P-rich limit is when $\mu_P = \mu_P^{P-bulk}$ while the Ga-rich limit corresponds to case when $\Delta\mu_P$ is equal to the GaP heat of formation (ΔH_f (GaP) = −0.928 eV) which has been calculated with the black phosphorus phase and the orthorhombic α-Ga phase.[47,48] A detailed explanation of the computational part is presented in the Supporting Information.

For the Ga-rich limit, the most stable reconstruction is the Ga-rich GaP(001)md(2×4) with a value of 52.9 meV Å^{-2} while in the P-rich limit the most stable one is the P-rich GaP(001) (2×4) with a value of 57.4 meV Å^{-2}. The GaP(114)A-$\alpha 2(2 \times 1)$ surface is thermodynamically more stable than the GaP(114) B-$\alpha 2(2 \times 1)$ surface, as already reported in previous works for the GaAs material. The GaAs(114)A surface energy was found to lie 3 meV Å^{-2} below the GaAs(114)B.[44] In the interval from Ga-rich up to $\Delta\mu_P = -0.70$ eV, then from -0.70 eV $< \Delta\mu_P < -0.16$ eV and finally from $\Delta\mu_P = -0.16$ eV to P-rich conditions, the lowest surface energies are the ones of Ga-rich GaP(001)md(2×4), GaP(114)A-$\alpha 2(2 \times 1)$, and P-rich GaP(001)(2×4), respectively. Overall, the surface energy of the GaP(114)A-$\alpha 2(2 \times 1)$ is the lowest over a wide $\Delta\mu_P$ intermediate range (almost 60% of the full $\Delta\mu_P$ range) as compared to the GaP(001) surface energies. However, to predict the possible destabilization of the (001) surface by (114)A faceting, one should consider $\gamma_{GaP(114)A-\alpha 2(2 \times 1)}/\cos(\theta)$ (dashed pink line in Figure 2), where $\Theta = 19.48°$ is the angle between the GaP(114) and the GaP(001) surfaces. We can see that this corrected surface energy is still lower than the GaP (001) ones in almost 30% of the full $\Delta\mu_P$ range (-0.60 eV $< \Delta\mu_P < -0.36$ eV), traducing a destabilization of the (001) surface by GaP(114)A-$\alpha 2(2 \times 1)$ faceting. In contrast, the GaP(114) B-$\alpha 2(2 \times 1)$ surface obviously cannot destabilize the (001) surface, in agreement with experimental observations.

We note that although the destabilization of the (001) GaP surface by (114)A faceting is predicted by DFT in homoepitaxy, it

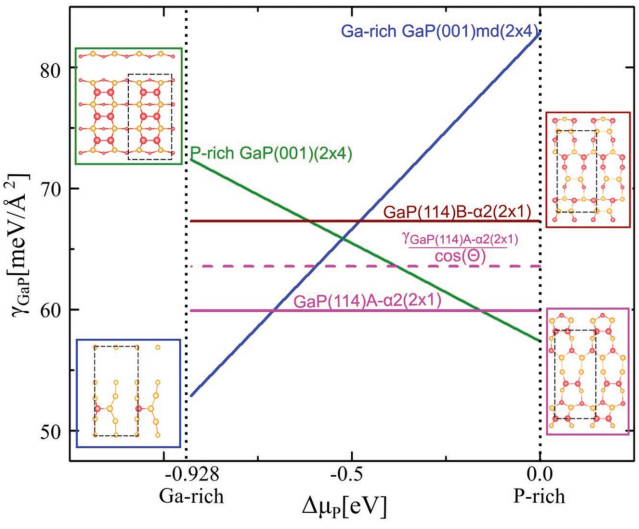

Figure 2. GaP surface energies γ versus the phosphorus chemical potential variation $\Delta\mu_P = \mu_P - \mu_P^{P-bulk}$. The dashed black lines represent the thermodynamic boundaries allowed for $\Delta\mu_P$: ΔH_f(GaP)[= −0.928 eV] $< \Delta\mu_P < 0$.

has not been experimentally observed on GaP substrate yet. This shows that the heteroepitaxial growth on the silicon substrate changes the surface energies balance. Note that a small shift of about +2 or −2 meV Å^{-2} in the surface energy of the (114) A or (001) surfaces, respectively, would be sufficient to inhibit the destabilization in the DFT prediction. This suggests that the destabilization regime is highly sensitive to small variations of surface properties. Although the relaxation degree of the GaP layer on Si is very high, a small residual stress induced by the heteroepitaxy cannot be ruled out and could explain why the destabilization was observed on Si and not on GaP substrates. An eventual anisotropic effect induced by vicinal Si substrates should be further investigated by comparisons of growth on vicinal and nominal substrates. We also point out that the GaP(001)-oriented surfaces on vicinal Si substrates were already obtained in previous works with different growth conditions.[26,49,50]

2.3. Textured GaP Surface over 2 in. Wafer and Its Benefits in the Water-Splitting Application

Even if a stress-free and textured GaP template on Si substrate has been obtained, the question of sample homogeneity is still raised, in the general context of a very large-scale integration. In order to check the homogeneity of the anisotropic surface texturation over a 2 in. wafer, optical surface control is the most efficient approach. For this aim, a 3 µm GaP/Si was grown in the same conditions as the 1 µm thick GaP/Si sample. Similar RHEED observations (streaky misoriented RHEED pattern) were obtained during the growth. The average distance between the ridges significantly increased, as compared to the 1 µm GaP/Si and reached 400 nm. Therefore, the pattern dimension becomes of the same order of magnitude that of the visible light wavelength.

To study the sample optical properties, we used as a reference object a metal box, labeled "INSA" (see **Figure 3**a,b). Then, the reflection/diffusion properties of light coming from this object are observed at the center of the sample surface. Ambient lightning is added, on the right side of the picture. Two pictures of the experiment performed exactly in the same conditions are given in Figure 3a,b. The same sample has been used in both figures, but the sample has been simply rotated by 90°. An arrow gives the Si [110] direction of the sample on both images. Two distinct areas are observed on this sample: (i) the central area of the sample that corresponds to nearly 90% of the total sample surface, starting from the center, and (ii) the crown area, corresponding to the edges of the sample (10% of the total sample surface on the outskirts of the sample). In the central area of the surface sample in Figure 3a, the edge of the metal box and the INSA logo are well and precisely reflected indicating that diffusion does not occur significantly. The sample appears mirror-like. If the sample azimuth is rotated by 90° (Figure 3b), a "milky" surface behavior appears indicating important contribution of light diffusion. These results suggest a strong and homogeneous anisotropy of surface texturation over 90% of the 2 in. sample. We then conclude that the central area of the sample is perfectly monodomain, and that {114}A textured surface has been obtained homogeneously over nearly 2 in.

Figure 3a,b also shows a more intriguing feature with this patterned surface. Indeed, for light parallel to [110], the central area appears mirror-like and the crown appears with a white "milky" behavior. On the opposite, when the light direction is along the [−110], the central area appears "milky," the crown appears mirror-like. This shows that a {114}A textured surface has also been obtained in the crown area, but its orientation is turned by 90°, as compared to the central area. These opposite light effects, at the center and at the edge of the sample, suggest that the majority domains developed in these two areas are different. These two areas are therefore in antiphase one for the other. A giant antiphase boundary is therefore expected at the separation between the central area and the crown area.

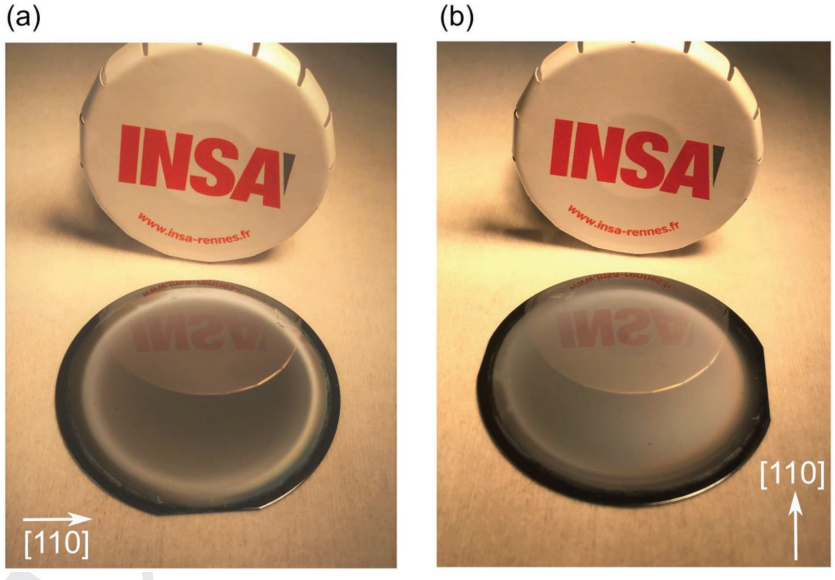

Figure 3. a,b) Study of light reflection on the 2 in. wafer of GaP(114)/Si 6°-off surface rotated by 90° with respect to (b).

We assume that the formation of these two different domains could be due to the inhomogeneity of growth temperatures and fluxes in the central area and in the crown area during the sample growth. Further works will be needed to clarify this finding. Nevertheless, a large-scale {114}A textured GaP surface has been successfully obtained in this work on a silicon substrate. We now discuss the relevance of GaP(114)A surfaces for water-splitting applications. Indeed, beyond the high thermal stability and the benefit of the free postprocessing aspect, there are other advantages in terms of optical and electrical devices properties inherent to the GaP material. First, the electric device properties can benefit from the GaP direct growth on Si substrate where the ohmic contact can be realized easily to connect an external circuit. Indeed, the realization of ohmic contacts on the GaP remains very challenging because of its large bandgap,[51] while for the Si substrate it is a well-known process which

simplifies the device fabrication. Moreover, the band lineup of the GaP/Si heterointerface is another advantage. Indeed, GaP and Si have a large bandgap difference ($E_g^{Si} = 1.12$ eV, $E_g^{GaP} = 2.26$ eV at 300 K) and their bandgap alignment is of type I favoring the extraction of the photogenerated carriers in the GaP photocatalyst through the Si substrate, when a potential is applied. We also point out that if GaP naturally fits photocathode requirements, quasi lattice-matched AlGaP[52] can also be grown on Si that lowers the alloy valence band to reach photoanode adapted band lineups.[53]

Finally, in the water-splitting reaction, the catalyst surface area plays an important role since it constitutes the main part where the oxidation occurs. It means that a stable and high catalyst surface area is beneficial for the water-splitting efficiency providing more active sites for the photocatalytic reaction.[40–43] Here, thanks to the surface texturation, a larger surface area has also been gained with respect to the planar one. The gain can be easily quantified since we know the GaP{114}A facets angle. The GaP (001) and GaP (114)A surface areas are linked with $S_{GaP(001)} = \cos\theta\, S_{GaP(114)}$, where $\cos\theta \approx 0.94$. Consequently, we expect a surface gain of 6%. Moreover, the textured surface may enable a more efficient light trapping into the material, where the direct expected consequence is an increase of light absorption which enhances the photogenerated carrier density.

3. Conclusions

A large-scale textured surface was achieved by growing micrometer-thick GaP layers on vicinal Si(001) substrates, thanks to the instability of the (001) GaP surface against (114)A faceting. This destabilization is also predicted by DFT calculations of GaP(001)(2 × 4), GaP(001)md(2 × 4), and GaP(114)A-α2(2 × 1) surface energies. We propose to use this surface energy engineering to develop large-scale textured GaP templates monolithically integrated on Si, for water-splitting applications. We believe that this nanopatterning approach could also benefit to various other applications, such as window layers in photovoltaic solar cells, nanofluidic applications, surface nanofunctionalization, or biologic sensors.

Supporting Information

Supporting Information is available from the Wiley Online Library or from the author.

Acknowledgements

The authors acknowledge Dr. J. Zhu for giving advices on DFT description of polar surfaces. This research was supported by the French National Research Agency Project ANTIPODE (Grant No. 14-CE26-0014-01). The ab initio simulations were performed on HPC resources of TGCC and CINES under the allocation 2017-[x20170906724] made by GENCI (Grand Equipement National de Calcul Intensif).

Conflict of Interest

The authors declare no conflict of interest.

Keywords

GaP/Si, nanopatterning, self-organization, textured surfaces, water splitting

Received: March 2, 2018
Revised: April 18, 2018
Published online:

[1] A. Fujishima, K. Honda, *Nature* **1972**, *238*, 37.
[2] M. G. Walter, E. L. Warren, J. R. McKone, S. W. Boettcher, Q. Mi, E. A. Santori, N. S. Lewis, *Chem. Rev.* **2010**, *110*, 6446.
[3] J. M. Ogden, *Annu. Rev. Energy Environ.* **1999**, *24*, 227.
[4] H. Li, Y. Zhou, W. Tu, J. Ye, Z. Zou, *Adv. Funct. Mater.* **2015**, *25*, 998.
[5] R. Marschall, *Adv. Funct. Mater.* **2014**, *24*, 2421.
[6] E. E. Barton, D. M. Rampulla, A. B. Bocarsly, *J. Am. Chem. Soc.* **2008**, *130*, 6342.
[7] B. Kaiser, D. Fertig, J. Ziegler, J. Klett, S. Hoch, W. Jaegermann, *ChemPhysChem* **2012**, *13*, 3053.
[8] D. Cedeno, A. Krawicz, P. Doak, M. Yu, J. B. Neaton, G. F. Moore, *J. Phys. Chem. Lett.* **2014**, *5*, 3222.
[9] M. Malizia, B. Seger, I. Chorkendorff, P. C. K. Vesborg, *J. Mater. Chem. A* **2014**, *2*, 6847.
[10] A. M. Beiler, D. Khusnutdinova, S. I. Jacob, G. F. Moore, *Ind. Eng. Chem. Res.* **2016**, *55*, 5306.
[11] O. M. Williams, J. W. Shi, M. J. Rose, *Chem. Commun.* **2016**, *52*, 9145.
[12] O. Supplie, M. M. May, H. Stange, C. Höhn, H.-J. Lewerenz, T. Hannappel, *J. Appl. Phys.* **2014**, *115*, 113509.
[13] B. C. Wood, E. Schwegler, W. I. Choi, T. Ogitsu, *J. Am. Chem. Soc.* **2013**, *135*, 15774.
[14] M. M. May, O. Supplie, C. Höhn, R. van de Krol, H.-J. Lewerenz, T. Hannappel, *New J. Phys.* **2013**, *15*, 103003.
[15] X. Zhang, S. Ptasinska, *Phys. Chem. Chem. Phys.* **2015**, *17*, 3909.
[16] J. Qiu, G. Zeng, P. Pavaskar, Z. Li, S. B. Cronin, *Phys. Chem. Chem. Phys.* **2014**, *16*, 3115.
[17] A. Standing, S. Assali, L. Gao, M. A. Verheijen, D. van Dam, Y. Cui, P. H. L. Notten, J. E. M. Haverkort, E. P. A. M. Bakkers, *Nat. Commun.* **2015**, *6*, 7824.
[18] J. Zhao, Y. Guo, L. Cai, H. Li, K. X. Wang, I. S. Cho, C. H. Lee, S. Fan, X. Zheng, *ACS Energy Lett.* **2016**, *1*, 68.
[19] Y. S. Jung, J. B. Chang, E. Verploegen, K. K. Berggren, C. A. Ross, *Nano Lett.* **2010**, *10*, 1000.
[20] Y. Shin, S. Lee, *Nano Lett.* **2008**, *8*, 3171.
[21] W. Lu, D. Kim, *Nano Lett.* **2004**, *4*, 313.
[22] C. Teichert, *Phys. Rep.* **2002**, *365*, 335.
[23] B. Turan, J.-P. Becker, F. Urbain, F. Finger, U. Rau, S. Haas, *Nat. Commun.* **2016**, *7*, 12681.
[24] P. Guillemé, M. Vallet, J. Stodolna, A. Ponchet, C. Cornet, A. Létoublon, P. Féron, O. Durand, Y. Léger, Y. Dumeige, *Opt. Express* **2016**, *24*, 14608.
[25] C. Robert, C. Cornet, P. Turban, T. Nguyen Thanh, M. O. Nestoklon, J. Even, J. M. Jancu, M. Perrin, H. Folliot, T. Rohel, S. Tricot, A. Balocchi, D. Lagarde, X. Marie, N. Bertru, O. Durand, A. Le Corre, *Phys. Rev. B* **2012**, *86*, 205316.
[26] K. Volz, A. Beyer, W. Witte, J. Ohlmann, I. Németh, B. Kunert, W. Stolz, *J. Cryst. Growth* **2011**, *315*, 37.
[27] Y. P. Wang, A. Letoublon, T. N. Thanh, M. Bahri, L. Largeau, G. Patriarche, C. Cornet, N. Bertru, A. Le Corre, O. Durand, *J. Appl. Crystallogr.* **2015**, *48*, 702.
[28] T. Quinci, J. Kuyyalil, T. N. Thanh, Y. P. Wang, S. Almosni, A. Létoublon, T. Rohel, K. Tavernier, N. Chevalier, O. Dehaese, N. Boudet, J. F. Bérar, S. Loualiche, J. Even, N. Bertru, A. L. Corre, O. Durand, C. Cornet, *J. Cryst. Growth* **2013**, *380*, 157.

[29] N. Esser, U. Resch-Esser, M. Pristovsek, W. Richter, *Phys. Rev. B* **1996**, *53*, R13257.
[30] T. Yamada, H. Yamaguchi, Y. Horikoshi, *J. Cryst. Growth* **1995**, *150*, 421.
[31] J. Márquez, P. Kratzer, L. Geelhaar, K. Jacobi, M. Scheffler, *Phys. Rev. Lett.* **2001**, *86*, 115.
[32] A. Ponchet, A. L. Corre, A. Godefroy, S. Salaün, A. Poudoulec, *J. Cryst. Growth* **1995**, *153*, 71.
[33] F. Tinjod, B. Gilles, S. Moehl, K. Kheng, H. Mariette, *Appl. Phys. Lett.* **2003**, *82*, 4340.
[34] F. Tinjod, I.-C. Robin, R. André, K. Kheng, H. Mariette, *J. Alloys Compd.* **2004**, *371*, 63.
[35] B. Damilano, N. Grandjean, F. Semond, J. Massies, M. Leroux, *Appl. Phys. Lett.* **1999**, *75*, 962.
[36] M. D. Pashley, *Phys. Rev. B* **1989**, *40*, 10481.
[37] S. Mirbt, N. Moll, K. Cho, J. D. Joannopoulos, *Phys. Rev. B* **1999**, *60*, 13283.
[38] K. Luedge, P. Vogt, O. Pulci, N. Esser, F. Bechstedt, W. Richter, *Phys. Rev. B: Condens. Matter Mater. Phys.* **2000**, *62*, 11046.
[39] H. Döscher, T. Hannappel, *J. Appl. Phys.* **2010**, *107*, 123523.
[40] O. Pulci, K. Lüdge, P. Vogt, N. Esser, W. G. Schmidt, W. Richter, F. Bechstedt, *Comput. Mater. Sci.* **2001**, *22*, 32.
[41] P. H. Hahn, W. G. Schmidt, F. Bechstedt, O. Pulci, R. Del Sole, *Phys. Rev. B* **2003**, *68*, 033311.
[42] A. M. Frisch, W. G. Schmidt, J. Bernholc, M. Pristovsek, N. Esser, W. Richter, *Phys. Rev. B* **1999**, *60*, 2488.
[43] J. Márquez, P. Kratzer, K. Jacobi, *J. Appl. Phys.* **2004**, *95*, 7645.
[44] R. D. Smardon, G. P. Srivastava, *Phys. Rev. B* **2005**, *72*, 035317.
[45] O. Romanyuk, T. Hannappel, F. Grosse, *Phys. Rev. B* **2013**, *88*, 115312.
[46] N. Moll, A. Kley, E. Pehlke, M. Scheffler, *Phys. Rev. B* **1996**, *54*, 8844.
[47] L. Cartz, S. R. Srinivasa, R. J. Riedner, J. D. Jorgensen, T. G. Worlton, *J. Chem. Phys.* **1979**, *71*, 1718.
[48] H. Curien, A. Rimsky, A. Defrain, *Bull. Soc. Fr. Mineral. Cristallogr.* **1961**, *84*, 260.
[49] T. J. Grassman, M. R. Brenner, S. Rajagopalan, R. Unocic, R. Dehoff, M. Mills, H. Fraser, S. A. Ringel, *Appl. Phys. Lett.* **2009**, *94*, 232106.
[50] A. C. Lin, M. M. Fejer, J. S. Harris, *J. Cryst. Growth* **2013**, *363*, 258.
[51] *Molecular Beam Epitaxy: From Research to Mass Production*, 2nd ed. (Ed: M. Henini), Elsevier, **2018**, ch. 31.
[52] R. Tremblay, J.-P. Burin, T. Rohel, J.-P. Gauthier, S. Almosni, T. Quinci, A. Létoublon, Y. Léger, A. Le Corre, N. Bertru, O. Durand, C. Cornet, *J. Cryst. Growth* **2017**, *466*, 6.
[53] C. G. Van de Walle, J. Neugebauer, *Nature* **2003**, *423*, 626.
[54] S. Licht, B. Wang, S. Mukerji, T. Soga, M. Umeno, H. Tributsch, *J. Phys. Chem. B* **2000**, *104*, 8920.
[55] K. T. Fountaine, H. J. Lewerenz, H. A. Atwater, *Nat. Commun.* **2016**, *7*.
[56] W. Jiang, X. Jiao, D. Chen, *Int. J. Hydrogen Energy* **2013**, *38*, 12739.
[57] Z. Zou, J. Ye, K. Sayama, H. Arakawa, *Nature* **2001**, *414*, 625.

Editorial Office:
Wiley-VCH Verlag
Boschstraße 12, 69469 Weinheim
Germany

Tel.: (+49) 6201 606 531
Fax: (+49) 6201 606 500

Email: afm@wiley-vch.de
http://www.afm-journal.com

Reprint Order Form 2018

Short DOI: adfm. _____

Please send me and bill me for

☐ **Reprints** via ☐ airmail (+ 25 Euro)
☐ surface mail

Please send me and bill me for a:

☐ **Issue copies** (25 Euro)

☐ **high-resolution PDF file** (330 Euro).

My Email address:

_____

Please note: It is not permitted to present the PDF file on the internet or on company homepages.

Information regarding VAT

Please note that from German sales tax point of view, the charge for **Reprints, Issues or Posters** is considered as **"supply of goods"** and therefore, in general, such delivery is a subject to German sales tax. However, this regulation has no impact on customers located outside of the European Union. Deliveries to customers outside the Community are automatically tax-exempt. Deliveries within the Community to institutional customers outside of Germany are exempted from the German tax (VAT) only if the customer provides the supplier with his/her VAT number. The VAT number (value added tax identification number) is a tax registration number used in the countries of the European Union to identify corporate entities doing business there. It starts with a country code (e.g. FR for France, GB for Great Britain) and follows by numbers.

VAT no.: _____

(Institutes / companies in EU countries only)

Purchase Order No.: _____

Delivery address / Invoice address:
Name of recipient, University, Institute, Street name and Street number, Postal Code, Country

_____

_____

_____

_____

_____

_____

_____

Date and Signature: _____

Credit Card Payment (optional) -You will receive an invoice.

VISA, MasterCard, AMERICAN EXPRESS

Please use the Credit Card Token Generator located at the website below to create a token for secure payment. The token will be used instead of your credit card number.

Credit Card Token Generator:
https://www.wiley-vch.de/editorial_production/index.php

Please transfer your token number to the space below.

Credit Card Token Number

Price list for reprints (The prices include mailing and handling charges. All Wiley-VCH prices are exclusive of VAT)

No. of pages	Price (in Euro) for orders of 50 copies	100 copies	150 copies	200 copies	300 copies	500 copies
1-4	345	395	425	445	548	752
5-8	490	573	608	636	784	1077
9-12	640	739	786	824	1016	1396
13-16	780	900	958	1004	1237	1701
17-20	930	1070	1138	1196	1489	2022
for every additional 4 pages	147	169	175	188	231	315

Wiley-VCH Verlag GmbH & Co. KGaA; Location of the Company: Weinheim, Germany;
Trade Register: Mannheim, HRB 432833, Chairman of the Board: Mark Allin
General Partner: John Wiley & Sons GmbH, Location: Weinheim, Germany
Trade Register Mannheim, HRB 432296,
Managing Directors: Sabine Steinbach, Dr. Guido F. Herrmann

WILEY-VCH